INDUSTRIAL APPLICATION OF CONCENTRATED SOLAR HEAT: EXERGY ANALYSIS OF A THEORETICAL IRON-ETHYLENE PRODUCTION PROCESS

William R. Sheline, Timothy L. Hurst, Sheldon M. Jeter
Georgia Institute of Technology
Atlanta, GA USA
wsheline3@mail.gatech.edu

ABSTRACT

Concentrated Solar heat can reach very high temperatures and is thus better suited for high temperature industrial applications rather than lower temperature Rankine cycle electricity generation. One potential application is in the production of chemical or metal products such as ethylene (a feedstock for polymers) and iron. The optimal temperature to form both of these products is in the range 750-950°C which makes them much more suited to use the high temperature heat collected by a Concentrated Solar Heat Supply System (CSHSS) than electricity generation. A theoretical process that links the production of ethylene and iron was devised to allow for clean production of iron and ethylene from ethane, iron ore (hematite) and solar heat. A model was created using ASPEN PLUS software. In addition to a 1st law and 2nd law thermodynamic analysis of the process, a combined law exergy analysis was calculated to assess the potential work of each stream (stream exergy) and the amount of potential useful work destroyed by each component (exergy destruction). The calculation of the stream exergy and exergy destruction of every component shows the highest exergy destruction in the heat exchanger, and the second highest in the ethane reactor. The split exergy destruction indicates a small work input requirement to separate the hydrogen.

1. INTRODUCTION

Concentrated solar technologies use various means to collect and concentrate solar radiation for electricity generation or other industrial purposes. One of the more prevalent concentrating technologies is the Concentrated Solar Power Tower (CSPT). A CSPT includes three main components: the heliostat field, the solar receiver, and the central tower. The heliostat field is a field of (generally) thousands of flat mirrors that track the sun and reflect the sunlight on the solar receiver. By having thousands of heliostats reflecting sunlight on a single point, the sunlight is normally concentrated at least 2000-3000 times. This solar receiver is positioned at the top of the central tower. With this high intensity solar radiation, the solar receiver must be designed to withstand high thermal stresses and high temperatures while also having a high absorptivity and having the ability to transfer heat to a heat transfer fluid. The central tower acts as a support structure to lift the receiver off the ground while also being a housing for various heat exchangers, turbines, pumps and other machinery necessary for the conversion of the thermal heat into electricity or other products.

Due to 2nd law considerations, concentrated solar heat is best used for high temperature industrial applications. Although a prevalent use of the CSHSS is for electricity generation, the relatively low temperature Rankine Cycle does not take full advantage of the high temperature capabilities of the Concentrated Solar Heat. Rankine Cycles operate around 500°C while Concentrated Solar Heat reaches temperatures of 1300°C and has the potential to reach even higher temperatures as solar receiver technology is improved. A better application for the Solar Heat is in industrial applications that require heat around 1000°C. A major area of interest is in chemical process applications. This includes applications ranging from production of quicklime to hydrogen to metals such as Zn and Mg.[1,2] Unfortunately, the temperature and amount of heat required by each chemical process is different for every application. Some applications require large amounts of low temperature heat while others require high temperature heat while still others produce heat. This gamut of heat requirements makes it difficult to find an industrial chemical processing application that maximizes the potential of the heat supplied by the CSHSS.

2. THE IRON – ETHYLENE PROCESS

$$C_2H_6 \rightarrow C_2H_4 + H_2 \quad (1)$$

$$Fe_2O_3 + 3H_2 \rightarrow 3H_2O + 2Fe \quad (2)$$

This proposed production process uses a CSHSS as a heat source to produce ethylene from ethane and iron from iron ore. Equation 1 shows the splitting of ethane into hydrogen and ethylene, and Equation 2 is the reduction of iron ore into iron. As seen in equation 1, the production of ethylene

produces hydrogen as a byproduct. The hydrogen from the ethylene hydrocracking operation can be used as a reducing agent in the iron ore reduction process. Both of these reactions are endothermic and require significant heat input to support the reaction. Normally this required level of energy input is generated by the burning of fossil fuels which have a cost associated with them and are subject to significant price fluctuations. Replacing the fossil fuel energy input with solar energy has the potential to: eliminate the required cost and risk associated with fuels, reduce capital cost of combustion equipment, and reduce pollution by being a completely clean and sustainable technology while producing high value iron and ethylene products (with the additional valuable byproduct of water).

The heat is produced by utilizing a concentrated solar receiver tower with the ability to store thermal energy. This stored thermal energy will allow for the ethylene and iron production processes to operate beyond the normal hours of available sunlight. The stored thermal energy will be used to provide the thermal energy required by the two endothermic reactions. Two main products will be produced: Ethylene, a chief component in the production of plastics, and pig iron, the main component for making steel.

A visual overview of this cycle can be seen in Figure 1. The heat input will be used at several locations in the production process. First, the ethane is preheated in the ETHAPRE component. Next, the ethane is reacted to produce ethylene and hydrogen in the ETHCRACK component. After separation in the SPLIT component, the ethylene can be sold and the hydrogen can be heated in the HYDPRE component before being transferred to the iron production process. With the addition of heat from a heat transfer fluid, the hydrogen can reduce the iron ore in the IRONRXN to produce water and iron. The iron ore used in this reactor will be preheated in OREPRE. Similar to the ethylene process the solid iron will need to be separated from the other products of the reaction.

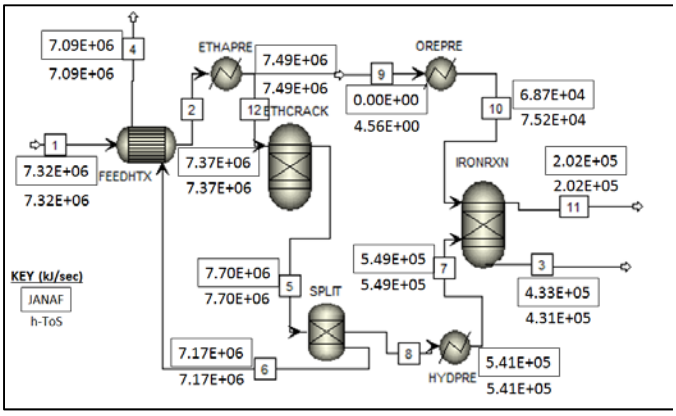

Fig. 1: Aspen Diagram with Stream Exergy Results

2.1 Ethylene Production

Heat is required for two parts of the traditional ethylene production process. First, the ethylene reaction has a positive change in enthalpy and thus the reaction requires heat (endothermic reaction). Second, the separation process requires heat to separate the ethylene from the other products. For the proposed plant design, thermal energy will be collected from the solar plant and stored in sand. From there, a heat exchanger will be used to transfer the heat to the ethylene and iron processes. The use of steam as a working medium between the sand and ethylene or iron process is also a viable option for thermal energy transmission that could allow for easier integration of the different systems. Once the heat as transferred to the ethylene process, ethane will be preheated and then reacted to form ethylene and hydrogen. This reaction can be seen in Equation 1. Other byproducts will also be formed such as unprocessed ethane, and methane. The unprocessed ethane, once separated, can be recirculated to prevent waste. The hydrogen can be separated via membrane separation and utilized for the iron reduction process.

Membrane separation will negate the need for the large quantities of thermal energy that is required in current industrial separation processes. The relatively small size of the hydrogen molecules compared to other products in the stream makes membrane separation more feasible. Once the hydrogen is separated from the ethylene process, it will be input into the iron reduction process. The pure, high temperature hydrogen can be used to reduce the iron ore into iron at much lower temperature than the current direct reduction methods, while keeping the same benefits of this process including: low maintenance… etc equipment etc. The already high temperature hydrogen will also reduce the energy input by reducing the thermal energy needed for the preheating stage. The utilization of the already high temperature hydrogen prevents the waste of useful thermal energy that can be conserved and stored for production during night hours.

2.2 Iron Production

As already mentioned, iron ore can be reduced into iron metal by utilizing the hydrogen produced from the ethylene production process. The stoichiometric equation for iron reduction with hydrogen is shown in Equation 2. As with the ethylene production this is an endothermic reaction which requires heat from the CSPT. The expected products from this reaction include hydrogen, water, iron metal and several iron oxides including magnetite (Fe_3O_4), hematite (Fe_2O_3) and ferrite (FeO). With exception of the water and hydrogen, all of the products will be in the solid phase and the iron will need to be separated from the unprocessed

iron ore and other iron oxides. A potential separation process could use a conventional method that uses Iron's lower melting temperature. The products could be reheated to melt the iron ore and the liquid iron could easily be separated from the other solid products. The iron reduction process will obtain the needed thermal energy input via sand as with the ethylene production process.

The most developed current processes for creating iron uses the direct reduction of iron from iron ore.[3] The process mixes iron ore and coal in a single chamber combustor. The coal is partially combusted to create carbon monoxide and heat. The carbon monoxide acts as a reducing agent to reduce the iron ore into iron at high temperature (~1400-1600°C) while also producing carbon dioxide. This process has the advantage over the hydrogen based method of being a simpler process and having lower capital costs. However, the direct reduction process (along with all previous processes) also produces slag and inadvertently produced coke resulting from the use of coal. The coking causes large buildups that require the plant to be shut down for maintenance. A similar process that uses hydrogen to reduce the iron ore would have all the advantages of the direct reduction process, but would have many added benefits. Using the proposed plant design utilizes lower reaction temperatures (as low as 500-600°C), which allows less costly materials to be used and increases the plant life. Since coal is no longer required for the iron reduction process coking and slag will no longer be of concern, the maintenance time and cost of cleaning the iron production equipment will be eliminated. The use of the solar energy as the thermal energy input also prevents the necessity for expensive combustion exhaust scrubbing equipment that may be necessary depending on local laws and regulations. The inherent clean nature of the process also provides a marketing advantage over other ethylene and iron reduction producers that utilize the current fossil fuel dependent processes.

The direct reduction of iron ore using hydrogen has been successfully demonstrated and has been proposed as a cleaner, less maintenance intensive, lower temperature alternative to the use of coal.[4] However, the proposed system has not been adopted by industry because a source of hydrogen is generally not available. In this situation, hydrogen is created in the ethylene process which can be readily used in the reduction of the iron. Alternatively, if only a decouple iron process was desired hydrogen could be produced using solar thermal energy and a small amount of methane in the well-developed steam methane reformation process. With a secure supply of hydrogen, the hydrogen and iron ore can be mixed and heated with thermal energy supplied by solar thermal storage to create iron through the endothermic reduction reaction in Equation 2. Because the temperature of this process is much lower, the iron will be created in the solid phase. This requires research into separation process to separate the iron from the iron ore. This separation could incorporate the use of further concentrate solar heat to melt the iron and separate it from the other products.

This system is still in the theoretical stage of design development, but this paper focuses on the exergy analysis of the system and specifically the methods that we used. Work will continue to optimize system for efficiency and output. These actual exergy values may change over time due to system modifications, but the methods that we use to determine them will stay the same.

3. EXERGY THEORY INTRODUCTION

In any design stage analysis, finding the efficiency of the process is important. It is important to know how much product will be produced at what cost. Several different measures exist for determining the efficiency of each component in a process, but the best measure is generally a measure of the exergy of the system (also known as the availability). Most measures of efficiency only include the 1^{st} law energy balance and ignore the very important 2^{nd} law considerations. On the other hand, the 2^{nd} law entropy analysis normally yields results that are hard to interpret and apply to an actual physical system. An exergy analysis combines both the 1^{st} and 2^{nd} laws to allow for complete and intuitive efficiency results. The exergy analysis finds the theoretical maximum amount of work that can be produced by a given stream and a reference medium (usually taken to be the atmosphere). This theoretical maximum amount of work called the "stream exergy" can then be used to find the amount of potential work destroyed by each process. This potential work destruction, called the exergy destruction, can be related to the entropy generation of the system and indicates the loss or inefficiency of a given component.

The derivation of the exergy equation includes two main parts: the thermo-mechanical exergy and the chemical exergy. The thermo-mechanical exergy includes all of the pressure and heat exergy of the system i.e. all of the work that could be generated from heat and pressure differentials. The chemical exergy includes all of the work that can be produced through a chemical reaction. For example, in a fuel cell, H_2 and O_2 are reacted to generate electrical work and H_2O. The theoretical development for both the thermo-mechanical and chemical exergy is explained in the next.

First, the thermo-mechanical exergy can be found by combining the 1^{st} law shown in Equation 3 with the 2^{nd} law shown in Equation 4. In these equations, both the heat rate,

$\dot{Q}$, and the net-work, $\dot{W}$, use the convention of in being positive, but include energy flow both into and out of the control volume.

$$\frac{dE}{dt} = \sum_{in} \dot{m} H_{GT} - \sum_{out} \dot{m} H_{GT} + \sum_{i=1}^{n} \dot{Q}_{in,i} + \dot{W}_{in} \qquad 3$$
$$h_{GT} \equiv h + \frac{V^2}{2} + gz$$

$$\frac{dS}{dt} = \sum_{in} \dot{m} s - \sum_{out} \dot{m} s + \sum_{i=1}^{n} \frac{\dot{Q}_{in,i}}{T_i} + S_{gen} \qquad 4$$

The goal of combining the two equations is to find the maximum amount of useful work available in any given arbitrary stream. Again, for the thermo-mechanical exergy, the stream has the restriction of no chemical reaction occurring. First, recognize that the useful work does not include any work on the medium by expansion of the control volume as shown in Equation 5. This causes $\dot{W}_{in}$ to be modified by $P_o \, dV/dt$. Then, Equation 6 can be found by multiplying the entropy equation by the temperature of the medium, T_o, and adding the energy equation. The final result shows the actual useful thermo-mechanical work available in a stream. Also, the S_{gen} term is defined as $\dot{I}$, the exergy destruction.

$$\dot{W}_{use} = \dot{W}_{in} - P_o \frac{dV}{dt} \qquad 5$$

$$\dot{W}_{act,use} + \frac{d(E + P_o V - T_o S)}{dt} = \sum_{in} \dot{m} (h_{GT} - T_o s) \ldots$$
$$\ldots - \sum_{out} \dot{m} (h_{GT} - T_o s) - \sum_{i=1}^{n} \dot{Q}_{in,i} \left(1 - \frac{T_o}{T_i}\right) + T_o S_{gen} \qquad 6$$
$$\dot{I} \equiv T_o S_{gen}$$

To find the goal of the maximum possible work that is available in the stream, we assume the process to be internally reversible and setting S_{gen} equal to 0. This reduces Equation 6 to the stream exergy of the system shown on the right hand side.

The chemical exergy is found by relating the chemical potential of the stream to the chemical potential of the medium. This exergy finds the available work of a system caused by a chemical reaction. For example, a fuel cell generates electrical work completely from the available chemical exergy stored in the inlet hydrogen and oxygen. The chemical exergy is found by finding the chemical potential of the stream at the temperature and pressure of the medium (the "frozen dead state") and comparing it to the chemical potential of the medium. It is also important to remember that the stream can contain multiple chemical species, so the chemical exergy of each chemical species will need to be calculated and summed to find the chemical exergy of the entire stream. Equation 7 shows the complete stream exergy of the system. In Equation 7, the properties have been switched to molar properties to avoid complicating the equation with multiple molecular weights, and the chemical exergy of the medium has been added to the thermo-mechanical exergy from Equation 6. Here, the reference state of the thermo-mechanical exergy for the enthalpy and entropy is assumed to be the same as the frozen dead state, allowing them to cancel. It is important that a consistent reference be used for both the frozen dead state and the reference relative dead state or else Equation 7 becomes longer and more complicated than the simplified form shown here. Also, for our system, we are assuming a steady state problem which eliminates the transient derivative on the left hand side. Finally, to find the maximum possible reversible work, the exergy destruction must be equal to zero.

$$\dot{W}_{act,use} = \sum_{in} \sum_{k} \dot{N}_k (\overline{H}_{GT,k} - T_o \overline{s}_k - \mu_k^0) - \cdots$$
$$\cdots \sum_{i=1}^{n} \dot{Q}_{in,i} \left(1 - \frac{T_o}{T_i}\right) \qquad 7$$

For any chemical species that exists in the medium, the chemical potential of the medium can easily be found by finding the molar Gibbs property. However, species such as ethane (C_2H_6) have no component in the medium and thus require a different method to find their respective potential. The μ_k^0 of any chemical species not present in the medium is considered to be a "fuel" and requires the calculation of the "fuel exergy". The chemical potential of these species is found by finding a system of chemical equations that relates the "fuel" to the chemical species in the atmosphere. For example, ethane can be related to the species in the medium (O_2, H_2O, CO_2) through its combustion reaction. The generalized fuel exergy is shown in Equation 8. For more in-depth development of the exergy equations see Wark chapter 3.[5]

$$\mu_{fuel} = (-\mu_{R1} \upsilon_{R1} - \mu_{R2} \upsilon_{R2} - \cdots + \mu_{P1} \upsilon_{P1} + \cdots) \qquad 8$$

4. EXERGY ANALYSIS-CH4 COMBUSTION

These exergy equations were used in conjunction with the ASPEN PLUS model to develop an exergy model including the stream exergy of each stream and the exergy destruction of each component. To validate both the results from ASPEN and the exergy calculations, a simple methane combustion model was developed using both the ASPEN PLUS software and using hand calculations solved with Engineering Equation Solver (EES). A schematic of the model is presented below in Figure 2.

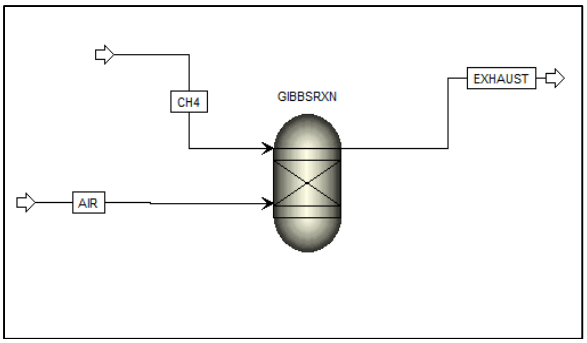

Fig. 2: CH4 Simulation Diagram

To model the methane combustion process, a simple Gibbs reactor with two separate inlets was utilized. The model has two inlets: the air stream containing pure oxygen with 0.5 excess oxidizer, and the fuel source of pure methane. Both inlets were at the reference temperature of 298K, the reference pressure of 1 bar, and in the vapor phase. The reactor was set to operate at 1000K. The exit stream left the system at the reactor temperature and with all components in the stream in thermodynamic equilibrium. The results from the ASPEN PLUS stream properties was used to calculate the stream exergy values. Using these values and the Q output determined during the simulation, the exergy destruction of the system was determined.

The two APSEN based models utilized the internal entropy and enthalpy data. The AVAIL function automatically calculates the Gibbs property (h-$T_0 \cdot s$) for each of the streams. To verify the AVAIL function, ASPEN's stream exergy function, within ASPEN PLUS we used the enthalpy and entropy values to manually determine the stream exergies. The enthalpy and entropy values were extracted from the model and the Gibbs property was calculated using simple hand calculations. These results matched the outputs from the AVAIL function for the pure substance inlet streams, but varied by around 9% for the mixed exhaust stream.

After finding the stream exergies using ASPEN, EES was used to perform verification hand calculations. The EES's internal thermodynamic data from the NIST JANAF tables was used to calculate the thermodynamic equilibrium, the Gibbs property, the Q exergy, the g_{medium}, and the overall stream exergy of each stream. All the components of the exergy analysis were calculated with two separate versions of code to verify the accuracy of the calculations. Both of the EES codes yielded the same results within a small margin of error. This yielded four separately derived sets of data: two from the ASPEN software, and two from the EES code. The stream exergy between the four models was compared with our previously verified EES model we calculated the difference between each model. Table 1 presents our results from this simulation.

This agreement between models indicates that ASPEN PLUS's internal entropy and enthalpy functions were working properly and gave us confidence that we had the correct process to determine the stream exergy. This calculation process could then be applied to the much more complicated Iron-Ethylene production process. The more complicated Iron-Ethylene process would create addition problems due to the multiple phases, multiple components and mixed stream states, but this model allowed for the solution of many issues with the software and calculations before dealing with the larger process.

TABLE 1: CH4 SIMULATION RESULTS

Exergy	Units	Aspen AVAIL	Aspen H-ToS	EES 1	EES 2 (JT)
O2 Stream	kJ/sec	11,861	11,861	11,867	11,867
Fuel Stream	kJ/sec	829,696	829,718	829,615	829,615
Exhaust Stream	kJ/sec	130,005	120,230	119,731	119,835
Q exergy	kJ/sec	-494,776	-494,776	-494,681	-494,861
Exergy Destroyed	kJ/sec	216,776	226,573	226,971	226,966

5. STREAM EXERGY ANALYSIS-IRON ETHYLENE PROCESS

The process learned through the simple methane combustion process was then applied to the more complex Iron-Ethylene production cycle. The stream exergy of each stream was calculated by finding the Q exergy, Gibbs free energy of each component in the medium, the total molar enthalpy, and total molar entropy assuming a steady state system. The stream exergy was calculated using three different methods to verify the results. The first method simply uses the enthalpy and entropy given in the results table of ASPEN to calculate the stream exergy. The second method uses the ASPEN AVAIL function. This function is a supposed short-cut that calculates h-To*s directly. Finally, the enthalpy and entropy of each stream was

calculated using the mole composition of each stream provided by ASPEN and an interpolation of the enthalpy and entropy at the given pressure and temperature provided by the NIST JANAF thermochemical data.[6] Inconsistency in the ASPEN AVAIL function was noticed for streams with multiple chemical species and thus produced invalid results. Good agreement between the JANAF and H-To*s results was achieved.

The complex nature of the system required that special attention be given to the phase related options within ASPEN. First, the equation of state for the entire process was selected to be the SRK model. The output was compared to the output for the WILSON equation of state, and no noticeable difference in the properties was observed. Next, ASPEN requires that the phase be specified in both the block and the stream (the phase is specified twice). In addition, it is not recommended to use the option allowing ASPEN to determine the phase. When using this option, the ASPEN software caused inappropriate phase changes that resulted in entropy values defying the 2nd law. These component blocks also had a difficult time analyzing the mixed state streams. On several occasions the presence of solids in a vapor stream skewed the results dramatically. To overcome this pure state streams were used with the assumption that phases would be separated within the reactor with no additional energy input.

Three main components were calculated to find the stream exergy of each stream. First, the H-To*S part was calculated as the total molar properties of the stream. This was done as a weighted molar average of each chemical species. Next, the Q exergy was calculated. The Q values were calculate using the 1st law balance on each component, and were compared to the Q values calculated by ASPEN as shown in Table 2. The Q values were very close and only differed by a small margin. The FEEDHTX and SPLIT had large percent difference, but this is due to the All of the preheaters were modeled as reversible heat input. The effective temperature of heat input was calculated as the change in enthalpy divide by the change in entropy. This caused all of the preheaters to be completely reversible and as expected, they had an exergy destruction of zero. Finally, the g_{medium} (or μ_k^0) was calculated using the enthalpy and entropy of each component. A medium composition was devised that uses the mole fraction of the gases in the atmosphere and assumes Fe_2O_3 to be present as a solid in the medium. The g_{medium} of each of these components was calculated and used to find the fuel exergy of Fe, C_2H_4, H_2, and C_2H_6.

TABLE 2: 1ST LAW ENERGY BALANCE

Component	Hout-Hin=Qin kJ/sec	ASPEN Q kJ/sec	% difference %
ETHAPRE	188715	188715	0.00
ETHCRACK	314730	314720	-0.003
FEEDHTX	0.0615	0.00	-100
SPLIT	-18.6	-15.0	-23.8
HYDPRE	10725	10723	-0.015
OREPRE	133821	133821	0.00
IRONRXN	20308	20363	0.270

6. RESULTS

Figure 1 shows the results of the stream exergy analysis. The stream exergies calculate by hand using the NIST JANAF table properties and the stream compositions from ASPEN are highlighted in boxes while the stream exergies calculated with the h-To*S method entirely from ASPEN properties and compositions are the numbers displayed without boxes. As seen in the figure, there is good agreement between the two methods for all streams. Streams 9 and 10 seem to have very large errors, but this only due to the much smaller magnitude of the exergies at these two states. Stream 10 has the largest difference, and this seems to be due to the slight difference in the enthalpy property calculated by the two methods. The stream exergy calculation require the calculation of three main components: the Gibbs property h-To*S, the g_{medium} of the stream, and the Q exergy of the stream.

The g_{medium} table is shown in Table 6. This table shows the composition used for the medium and the corresponding g_{medium} calculated per mole of species. The first five species are considered to be part of the medium, and the g_{medium} was calculated as the simple Gibbs property. The remaining four components were found using the chemical exergy. These chemical exergies were found through a system of four chemical equations shown below in Equations 9a-d.

$$2H_2 + O_2 \rightarrow 2H_2O \quad (9a)$$

$$Fe_2O_3 + 3H_2 \rightarrow 3H_2O + 2Fe \quad (9b)$$

$$2C_2H_6 + 7O_2 \rightarrow 4CO_2 + 6H_2O \quad (9c)$$

$$C_2H_6 \rightarrow C_2H_4 + H_2 \quad (9d)$$

The Gibbs property and the Q exergy were calculated using the enthalpy and entropy of each stream. The results of the

Q exergy is shown in Table 3. There were small deviations between the two methods, but overall the results were very consistent. The total shows the total theoretical Q exergy needed for this process is about 440 MJ (work)/kmol iron ore input (assuming a constant ratio of ethane input to iron ore input).

TABLE 3: COMPONENT Q EXERGY

Component	Q (h-ToS) kJ/sec	Q (JANAF) kJ/sec	Q exergy (h-ToS) kJ/sec	Q exergy (JANAF) kJ/sec
ETHAPRE	188715	188826	120779	120747
ETHCRACK	314730	314270	221652	221328
FEEDHTX	0.00	0.00	0.00	0.00
SPLIT	-18.6	0.00	-13.1	0.00
HYDPRE	10725	10748	7782	7806
OREPRE	133821	124702	75158	68727
IRONRXN	20308	32561	15125	24251
Total	668280	671107	440483	442858

The exergy destruction is also shown in Table 4. As expected, all of the preheaters had an exergy destruction of zero. This is due to them being modeled as reversible heat input. A future study will include a Q vs T diagram for exchanging heat between all of the components and calculate the additional exergy destruction due to the heat exchange between the CSHSS and the Iron-Ethylene production process. Additionally, as expected, the heat exchanger has the largest exergy destruction due to the inherent heat transfer irreversibility. The other interesting result is the negative exergy destruction of the splitter. This is not actually an exergy destruction, but is instead an indication of the work input that is required for the splitter to operate. This work input is required due to a pressure increase. The pressure of the inlet, and both of the outlet streams are all at the same pressure, resulting in an increase in the partial pressures of the various species.

The results for the exergy destruction were verified with a second law analysis shown in Table 7. The second law analysis calculates the exergy destruction via the entropy generation (S_{gen}) of the system shown in the bottom of Equation 4 above. The $T_{effective}$ of the system was calculated using the change in enthalpy over the change in entropy method. The stream entropy and Q entropy were added to find the S_{gen} of the system. The exergy destruction calculated with the exergy law and the exergy destruction calculated with the 2^{nd} law are compared in the last column, and there is little difference between the two methods, verifying the accuracy of the model.

Finally, Table 5 shows the result of a full system analysis. It treats the entire production process as one large component and calculates the Q exergy in, the stream exergy in, the total exergy into and out of the system, and the exergy destruction. Again, the exergy destruction from this overall balance matched the totaled exergy destruction in Table 4.

TABLE 4: COMPONENT EXERGY DESTRUCTION

Component	I (h-Tos) kJ/sec	I (JANAF) kJ/sec	I (h-ToS) % of Q exergy in	I (JANAF) % of Q exergy in
ETHAPRE	0.00	0.00	0.000	0.000
ETHCRACK	11695	11611	0.151	0.150
FEEDHTX	34721	34664	0.447	0.446
SPLIT	-10868	-10874	-0.140	-0.140
HYDPRE	0.00	0.00	0.000	0.000
OREPRE	0.00	0.00	0.000	0.000
IRONRXN	6632	7183	0.085	0.093
Total	42180	42583	0.823	0.829

TABLE 5: OVERALL CYCLE VALUES (h-ToS)

Q Exergy in	440483	kJ/sec
Stream Exergy in	7323989	kJ/sec
Total Exergy in	7764472	kJ/sec
Total Exergy Out	7722292	kJ/sec
Total Exergy Destroyed	42180	kJ/sec

7. CONCLUSION

This exergy analysis shows a small section of the design stage analysis being done to determine the technical feasibility of an industrial solar chemical reformation process. This paper shows the process and results for determining the steam exergy and exergy destruction of a Solar Iron-Ethylene production process. In addition to the exergy analysis, past analysis has included economic and energy payback studies, production rate calculations and yearly solar collection calculations.[7] The next step will include an exergy destruction study of the heat exchange between the CSHSS and the chemical process. This will include a Q vs T diagram and a comparison to the exergy destroyed by a typical Rankine cycle.

Although the cycle has not been optimized or scaled to a specific size, the general trends can still give insight into the behavior of the process. The stream exergies indicate that the areas of highest exergy are in the ethane cycle, and indicate a very large exergy leaving in stream 4. It will be important to find a use for this exergy in the optimization of the process either in recycling the products, or using them for another purpose. The exergy destruction of the splitter also shows the work requirement need for the hydrogen separation process. Finally, the analysis helped illuminate issues with the software program including the difficulty with the AVAIL function with mixed phase streams. As the project develops, this theoretical development can be integrated with future practical considerations (such as the efficiency of various components and cost) to make design stage estimates of production, fuel requirements, energy requirements and capital costs.

TABLE 6: MEDIUM COMPOSITION

Component	Mole Fraction	g=h-ToS (h-ToS) kJ/kmol	RTln(P*medium/P) kJ/(kmol*K)	G=g+RTln(P*/P) (h-ToS) kJ/kmol	G=g+RTln(P*/P) (JANAF) kJ/(kmol*K)
O2	0.203	-32.6	-3956	-3988	-65081
CO2	0.000	-394407	-19457	-413864	-476664
H2O	0.032	-228624	-8556	-237180	-306633
N2	0.756	-32.6	-693	-725	-57793
Fe2O3	1 (solid)	-742688	0.00	-742688	-851561
H2	N/A	N/A	N/A	-235186	-274093
FE	N/A	N/A	N/A	-368353	-376970
C2H6 (ethane)	N/A	N/A	N/A	-1525309	-1645445
C2H4 (ethylene)	N/A	N/A	N/A	-1290124	-1371352

TABLE 7: 2ND LAW ENTROPY BALANCE (h-ToS)

Component	Stream Sin-Sout kJ/sec*K	Teffective K	Q/T kJ/sec*K	Sgen kJ/sec*K	I=To*Sgen kJ/sec	Difference in I kJ/sec
ETHAPRE	-228	828	228	0.00	0.00	1.22E-11
ETHCRACK	-351	1008	312	39.2	11695	2.00E-11
FEEDHTX	-116	0.00	0.00	116	34721	6.15E-02
SPLIT	36.5	1008	-0.02	-36.5	-10868	-3.64E-12
HYDPRE	-9.87	1086	9.87	0.00	0.00	-5.30E-13
OREPRE	-197	680	197	0.00	0.00	0.00E+00
IRONRXN	-39.6	1168	17.4	22.2	6632	-5.28E-11

[1] Sheline W., et al., An Exploratory Study of the Solar Thermal Electrolytic Production of Mg from MgO, Energy. 2013.
[2] Schroeder R., et al., Solar Thermal Electrolytic Process for the Production of Zn from ZnO: The Electrolysis of AnO from 1275-1500 K. Journal of Solar Energy Engineering. 2011.
[3] Chatterjee, A. Sponge Iron Production by Direct Reduction of Iron Oxide. PHI Learning Private Limited. 2010.
[4] Chatterjee, A., Sponge Iron Production by Direct Reduction of Iron Oxide. PHI Learning Private Limited. 2010.
[5] Wark, K., Advanced Thermodynamics for Engineers. 1995, McGraw Hill,
[6] Chase, M. Jr., NIST-JANAF Thermochemical Tables Fourth Edition, Journal of Physical and Chemical Reference Data,
[7] Sheline, W., Said, A., Jeter, S. Concentrated Solar Power Tower: Energy and Economic Feasibility Study. ASME Early Career Technical Journal. American Society of Mechanical Engineers.